Journal of Materials Chemistry A

Accepted Manuscript

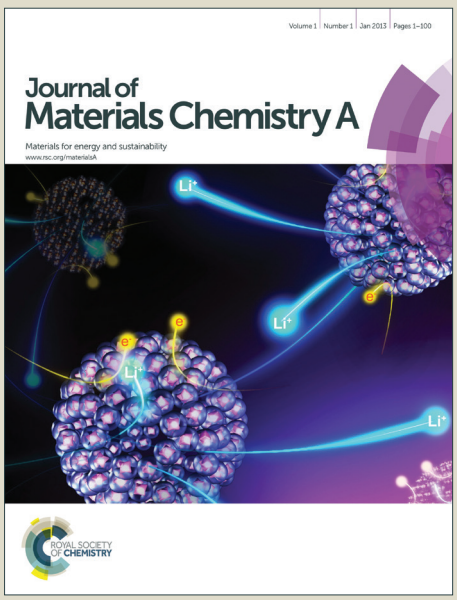

ROYAL SOCIETY OF CHEMISTRY

www.rsc.org/materialsA

Journal Name

RSCPublishing

ARTICLE

Synthesis and Characterization of Pure P2- and O3-$Na_{2/3}Fe_{2/3}Mn_{1/3}O_2$ as Cathode Materials for Na Ion Batteries

Cite this: DOI: 10.1039/x0xx00000x

Received 00th January 2012,
Accepted 00th January 2012

DOI: 10.1039/x0xx00000x

www.rsc.org/

E. Gonzalo,[a] M. H. Han,[a] J.M. López del Amo,[a] B. Acebedo,[a] M. Casas-Cabanas[a] and T. Rojo.[a,b,*]

The solid state synthesis and electrochemical characterization of pure P2- and O3-$Na_{2/3}Fe_{2/3}Mn_{1/3}O_2$ have been carried out. Both phases have been characterized with XRD, solid state NMR, and ICP techniques . The initial charge capacity of P2-phase reached 114.7 mAh/g and was followed by a discharge capacity of 151.09 mAh/g within the voltage range of 4.2 - 1.5 V at C/10. The capacity retention gradually decreased to 122.83 mAh/g at the 10th cycle, and then remained stable up to the 15th cycle. O3-phase resulted in a first charge capacity of 134.01 mAh/g with a discharge capacity of 157.47 mAh/g in the same experimental conditions. The capacity retention gradually decreased to 122.24 mAh/g at the 10th cycle but, as in the other polymorph, the capacity remained stable at least up to the 15th cycle. Although the voltage profile is slightly different, the overall electrochemical performance of both phases is shown to be very similar, which implies that, contrary to the common belief, the electrochemical performance of this compound does not highly depend on the layer stacking sequence adopted by the material.

Introduction

Li-ion batteries have enjoyed from an enormous success during the last two decades on portable electronic devices and now the demand is directed towards their widespread use in vehicular and stationary applications. However, due to the production cost of lithium and its limited geographic distribution, the use of Li-ion batteries may be limited to hand held devices or electric vehicles. Therefore, the awareness that cheaper and more accessible intercalation elements like sodium are needed (sodium is the 6th most abundant element on earth[1]), has recently directed researchers' attention towards Na-ion batteries. Although, in principle, Na-ion batteries cannot match the specific energy of Li-ion batteries because of lower operation voltages and heavier mass, Na-ion batteries may be considered to be a viable alternative to Li-ion batteries owing to their lower cost.[2,3]

One of the most promising family of cathode materials for Na-ion batteries is $NaMO_2$ layered oxides (M = Cr, Mn, Fe, Co, Ni, and mixtures of 2-3 transition metals) because of their high capacity and structural simplicity.[4,5] All layered oxides can be classified by the oxygen stacking sequence and surrounding environment for sodium.[6] Typical structural types for layered oxides are P2 and O3. In P2-phase, sodium is located in between the MO_6 oxide layers resulting in a $AB_{Na1}BA_{Na2}A$… pattern with sodium ions coordinated to oxygen atoms in a trigonal prismatic environment, one edge sharing and one face sharing (see Fig.1). In O3-phase, sodium ions are located between the oxide layers where oxygen stacking is in $AB_{Na1}CA_{Na2}BC_{Na3}A$… pattern in which each sodium is octahedrally coordinated to oxygen sharing one edge and one face with MO_6 octahedra.

It has been widely believed that P2-phase exhibits better overall electrochemical performance due to structural stability.[7] In fact, P2-$Na_{2/3}Fe_{1/2}Mn_{1/2}O_2$ phase delivers the highest charge/discharge capacity achieved by a Na-ion cathode material, reaching 190 mAh/g of reversible capacity in a sodium half-cell within the voltage range of 4.3 - 1.5 V.[8] In contrast, the O3-phase $NaFe_{1/2}Mn_{1/2}O_2$ could only produce approximately 110 mAh/g within the same voltage range.[9] It is worth noting that the sodium contents of these two P2 and O3 examples are different in their pristine state, and so are the iron and manganese oxidation states. Therefore, the different electrochemical behaviour of those phases may not only be due to the structural difference but also due to the oxidation state of the transition metals in the pristine state. In addition, it has been shown in the $Na_xFe_xMn_{1-x}O_2$ ($0.5 \leq x \leq 1.0$) system[10] that the P2-phase is obtained for Na values below 0.7 while the O3-phase would form above 0.7. In this report, the electrochemistry of P2-phases was shown to be better than that of O3-phases.[10] However, since both composition and structure in this system were different, their independent effect on electrochemistry could not be decoupled.

Here we report on the electrochemical performance of pure P2- and O3- $Na_{2/3}Fe_{2/3}Mn_{1/3}O_2$ phases synthesized by solid state route. For the first time a direct comparison of the electrochemical behaviour between the two polymorphs with identical Fe:Mn ratio is carried out. In order to try to increase the energy density of $Na_{2/3}Fe_{1/2}Mn_{1/2}O_2$[8], a 2/3:1/3 Fe:Mn ratio has been chosen to extend the $Fe^{3+/4+}$ voltage plateau. Both P2- and O3-phases exhibit similar electrochemical performance with capacity values over 150 mAh/g in the initial charge/discharge process which are comparable to those described in the literature[8,10,11] but, contrary to what is commonly believed, the overall electrochemistry turns out to be only slightly influenced by the stacking of the layers.

Experimental

The synthesis of P2-phase $Na_{2/3}Fe_{2/3}Mn_{1/3}O_2$ was carried out using the method described in the literature[12] slightly modified. A stoichiometric mixture of Na_2CO_3, Fe_2O_3, and Mn_2O_3 was ground in a planetary ball mill for 1 hour at 250rpm with 12mm diameter zirconia balls (1:20

active material:balls weight ratio) and pressed into pellets. Then, the pellets were fired at 1000ºC for 12 hours under 1 bar O_2 pressure followed by slow cooling.

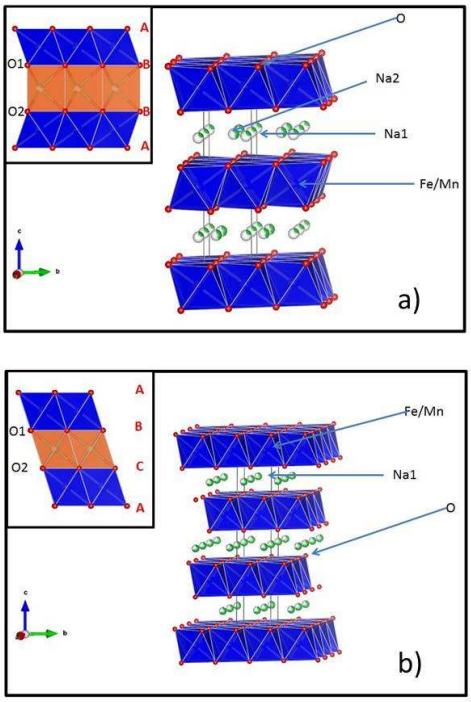

Fig. 1a) Schematic P2- and b) O3- structures of Na-Fe-Mn-O layered compounds. Insets show the different oxygen stacking.

The O3-$Na_{2/3}Fe_{2/3}Mn_{1/3}O_2$ phase was synthesized using a stoichiometric mixture of $NaNO_3$, $Fe(OH)_3$, and $Mn(OH)_2$ pelletized and heated under 1 bar O_2 atmosphere at 700ºC and 900ºC successively for 1 hour with intermediate grinding.

The XRD diffraction patterns were collected with a Bruker D8 Advance with Cu K_α radiation (λ = 1.5418 Å) within the 2θ range of 15 – 80º. All samples were mounted onto an atmosphere protective XRD sample holder with a Kapton film cover in order to avoid atmospheric moisture contact. Pattern matching was performed using FullProf software package[13], and VESTA (Visualization for Electronic and Structural Analysis) program[14] has been used to draw the different structures based on the structural data. Inductively Coupled Plasma Absorption Emission Spectroscopy, ICP-OES, was performed using the Horiba Scientific Ultima 2 spectrometer, and SEM measurements were carried out with FEI Quanta 250 microscope. ^{23}Na magic angle spinning nuclear magnetic resonance (MAS NMR) experiments were performed at 52.9 MHz, on a Bruker-300 spectrometer charged to a field of 4.7 T using a 1.3 mm MAS probe at rotor spinning speeds of 60 kHz. A rotor synchronized spin−echo pulse sequence (90°−τ−180°−τ1−acquisition) was used with typical 90° and 180° pulses of 1 and 2 µs, respectively, and a recycle delay of 0.4 s. The spectra were referenced to a 0.1 M solution of ^{23}NaCl.

Electrode preparation was performed in an Ar-filled glove box in order to avoid any atmospheric moisture contamination. The electrode slurry was prepared by a mixture of the active material, super carbon C_{65}, and PVdF (Polyvinylidene fluoride) as binder in the mass ratio of 80:10:10 in NMP (N-Methyl-2-pyrrolidone) followed by vigorous stirring for 2 hours. The slurry was then hand-casted onto an aluminium current collector sheet using a Dr. Blade. The laminate was immediately transferred into a vacuum oven and dried at 80ºC under constant vacuum for 12 hours before ½" circular individual electrodes were punched out. Na half-cells were constructed with $Na_{2/3}Fe_{2/3}Mn_{1/3}O_2$ laminate electrode/0.5M $NaPF_6$ in EC (ethylene carbonate):DMC (dimethyl carbonate)/Na in 2032 coin cells in the Ar-filled glove box. The galvanostatic electrochemical testing was performed with Bio-Logic VMP3 potentiostat within the voltage range of 4.2 – 1.5 V at C/10 rate at room temperature. Rate capability tests were done atC/10, C/7.5, C/5, C/2.5 and 1C.

Cycled cells were disassembled in the Ar-filled glove box to collect the electrodes for ex-situ XRD studies. The electrodes were thoroughly washed with DMC and dried under vacuum for at least 30 minutes before XRD investigation.

In situ XRD samples were prepared with a custom designed 1" *in situ* cell equipped with Be window for XRD observation in a polypropylene body. A powder mixture of active material and super carbon C65 at the weight ratio of 80:20 was loaded in the cell along with 2 glass fiber separators. A proper amount of 0.5M $NaPF_6$ in EC:DMC (1:1) electrolyte was added before closing the cell with a Na platted stainless steel plunger. The cell was galvanostatically cycled over the voltage range of 4.2 – 1.5 V at C/20 using a Biologic SP200 potentiostat. Each scan was collected in 0.02° increments between 15 -50º.

Results and discussion

Since it was previously believed that $Na_xFe_xMn_{1-x}O_2$ ($0.5 \leq x \leq 1.0$) compositions can only be isolated either in the P2-type ($x<0.7$) either in the O3-type ($x>0.7$)[10,15], a direct comparison of the electrochemical behaviour of P2- and O3-phases with identical chemical composition has not been reported to date. The P2-phase $Na_{2/3}Fe_{2/3}Mn_{1/3}O_2$ was synthesized with a single calcination process at 1000ºC for 12 hours under 1 bar O_2 pressure. Upon cooling to room temperature, a dark-brown fine powder is obtained. The O3-phase $Na_{2/3}Fe_{2/3}Mn_{1/3}O_2$ was obtained with a double calcination at 700ºC and 900ºC for 1 hour along with an intermediate grinding. The final product is lighter in colour than P2-phase probably because of milder synthesis condition and therefore, smaller particle size. It should be noted that both syntheses were carried out under 1 bar O_2 pressure in order to oxidize the Mn^{3+} cations in the precursor to Mn^{4+}.

Figures 2a) and b) show a general view of the morphology and size distribution obtained by Scanning Electron Microscopy of the pristine P2 and O3 materials. The SEM photographs reveal that P2 obtained by classical solid state route produces micrometric platelets with an average particle size of more than 5 microns (see inset Fig. 2a), while O3 phase shows an homogenous distribution of smaller disk-shaped particles with an average size of 1 micron maximum (see inset Fig. 2b). This particle size difference can be attributed to the different starting materials and calcination condition since it has been reported that solid state reaction with oxides as starting materials resulted in several micron size products, while solid state reaction with hydroxide as starting materials resulted in sub-micron size product.[16] Indeed, P2-phase is synthesized using a mixture of oxides at higher temperature and longer dwell time while O3-phase is synthesized using a mixture of nitrate and hydroxides at lower temperature and much shorter dwell time.

Elemental Analysis of Na, Mn and Fe has been performed by means of ICP-OES technique and the experimental values are in good agreement with the theoretical values as seen in table 1. It should be noted that under the synthesis conditions, the Na concentration of the pristine product remains the same as the starting stoichiometry even though no extra Na is used, which indicates that no appreciable amount of Na evaporation occurred during the synthesis even at 1000 ºC for 12 hours.

Table 1. ICP elemental analysis of P2- and O3- $Na_{2/3}Fe_{2/3}Mn_{1/3}O_2$.

	P2- $Na_{2/3}Fe_{2/3}Mn_{1/3}O_2$		O3- $Na_{2/3}Fe_{2/3}Mn_{1/3}O_2$	
Element	Theoretical value	Experimental value	Theoretical value	Experimental value
Na	0.67	0.68	0.67	0.68
Mn	0.33	0.34	0.33	0.32
Fe	0.67	0.67	0.67	0.67

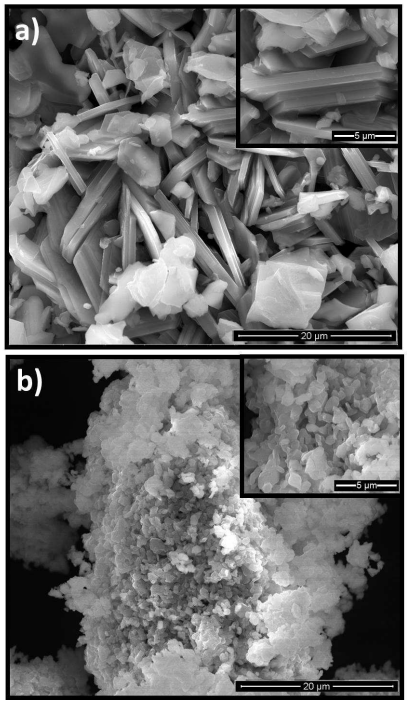

Fig. 2 SEM images of a) P2- and b) O3- $Na_{2/3}Fe_{2/3}Mn_{1/3}O_2$, insets show higher magnification pictures.

Figures 3a) and b) show the X-ray diffraction patterns of P2- and O3- $Na_{2/3}Fe_{2/3}Mn_{1/3}O_2$ respectively. X-ray diffraction pattern of P2- can be fully indexed with the hexagonal $P6_3/mmc$ space group (a= 2.9445(5) Å; c= 11.1778(3) Å) whereas O3- is indexed with the rhombohedral R-3m space group (a=2.9905(1) Å; c=16.2602(9) Å) (See Table 2). The a-parameter for both phases is similar to each other because the oxide layers are composed of analogous transition metals with the same composition. However, the c-parameter of the O3-phase is significantly larger than that of the P2-phase due to the fact that the number of layers in the unit cell are different[10] (2 layers for P2-phase and 3 layers for O3-phase). The interlayer distance calculated by VESTA software package indicates that the P2-phase has a slightly larger interlayer spacing (3.14 Å) than the O3-phase (2.71 Å). As seen in the inset in fig 1a), $AB_{Na}BA$ oxygen layer stacking of P2-phase imposes larger O-O repulsion because oxygen (O1) on one layer faces directly on top of the other oxygen of the adjacent layer (O2). Meanwhile, in O3 stacking, the interlayer distance is smaller because the oxygen atom of one layer (O1) is displaced 1/3 of the unit cell with respect to the next oxygen (O2) in the adjacent oxygen layer as seen in inset in fig 1b). As a consequence of the different space group and interlayer spacing, significant differences can be found in the XRD patterns. Indeed, the first diffraction peak ((002) for the P2-phase and (003) for O3-) appears in a slightly different position ($2\theta = 15.86^o$ and 16.34^o respectively). More significant differences are observed in the intensity of the peaks at higher angles. For instance, in the 30º - 45º 2θ range, P2-phase exhibits four Bragg diffraction peaks of similar intensity ((004) at 32.03^o, (100) at 35.17^o, (102) at 38.79^o and (103) at 42.95º) while in O3- diffractogram three Bragg diffraction peaks of similar intensity appear ((006) at 33.03^o, (101) at 35.06^o and (012) at 36.38^o) followed by a very intense reflection ((104) at 41.30º). In both phases, no structural distortion occurs which is due to the presence of high spin octahedrally coordinated Fe^{3+} ($t_{2g}^3e_g^2$) and Mn^{4+} ($t_{2g}^3e_g^0$) where no Jahn-Teller effect is present.

Table 2. Refined cell parameters of P2- and O3- $Na_{2/3}Fe_{2/3}Mn_{1/3}O_2$.

Cell parameters	P2	O3
a (Å)	2.9445(5)	2.9905(1)
c(Å)	11.1778(3)	16.2602(9)
α=β (°)	90	90
γ (°)	120	120
S.G.	P63/mmc	R-3m

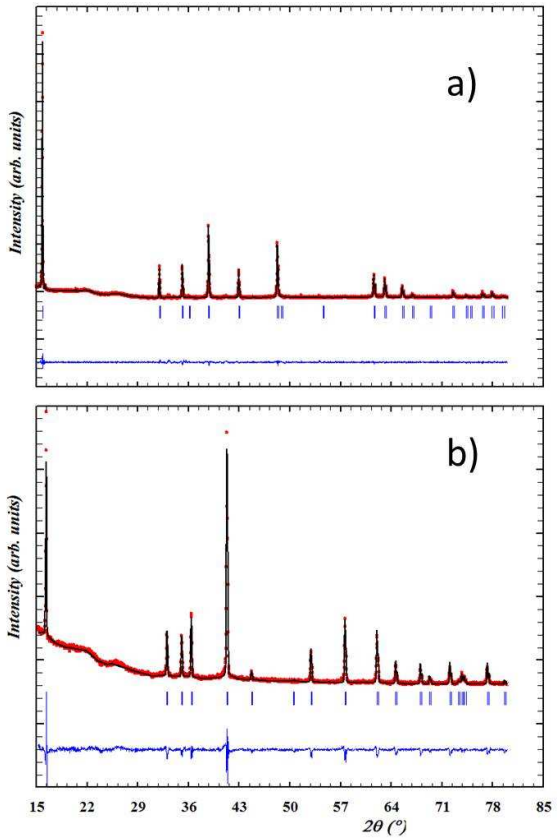

Fig. 3 X-ray diffraction patterns XRD pattern matching of a) P2- and b)O3- $Na_{2/3}Fe_{2/3}Mn_{1/3}O_2$ powder: experimental pattern (dotted curve), refined profile (continuous line), and Bragg positions (vertical bars).

The ^{23}Na solid-state MAS NMR spectra of microcrystalline P2-$Na_{2/3}Fe_{2/3}Mn_{1/3}O_2$ and O3-$Na_{2/3}Fe_{2/3}Mn_{1/3}O_2$ are shown in Fig. 4. The spectra were recorded at MAS frequencies as high as 60 kHz using a 1.3 mm rotor in a 4.7 T magnet in order to avoid interference of the central transition and the MAS satellite signals marked by "*" in the figure. ^{23}Na NMR shifts obtained for both samples are very large, as predicted by the presence of Na-O-M (M = Fe, Mn) hyperfine contacts with paramagnetic centers[17]. The larger shift, as estimated by the center of gravity of the signals, is observed for the O3 phase (3050 ppm) as

compared with the P2 (2450 ppm). This difference is in agreement with the changes expected in the Na-O-TM bond distances and angles that predict a shorter Na-O distance and Na-O-TM angles closest to the ideal 90 and 180º for the O3 phase, leading to a more effective overlap between the paramagnetic center and the ^{23}Na ions and to a stronger hyperfine interaction (see insets of Fig.4).[17] The small and narrow signal observed close to 0 ppm could be ascribed to the presence of a diamagnetic impurity such as Na_2CO_3. These impurities were not detected by XRD because they are present in very small amounts.

In principle, we would expect to observe two ^{23}Na signals in the NMR spectrum of P2- $Na_{2/3}Fe_{2/3}Mn_{1/3}O_2$ due to the existence of two crystallographic distinct sites for Na in the ideal structure.[8] The large 23Na NMR signal broadening induced by the strong magnetic behaviour of the sample, precluded the resolution of both signals in the P2 spectrum of Figure 4. It is also possible that the signal is affected by the presence of ion motion in the NMR timescale. In fact, Na^+ mobility was reported in P2-$Na_{2/3}Ni_{1/3}Ti_{2/3}O_2$ by NMR[18] and proposed for P2-$Na_{2/3}Ni_{1/3}Mn_{2/3}O_2$ [19]. The spectrum of O3-$Na_{2/3}Fe_{2/3}Mn_{1/3}O_2$ is characterized by a larger broadening as compared with the P2. Very large ^{23}Na MAS NMR signal broadening that expanded over almost 3000 ppm was observed previously in O3- $Na_{0.9}Ni_{0.45}Mn_{0.55}O_2$, while P2- $Na_{2/3}Ni_{1/3}Mn_{2/3}O_2$ resulted in a much narrower signal[19]. These results were interpreted based on the presence of extensive disorder in the O3 phase as compared with the P2 counterpart. Our results shown in Fig. 4 are qualitatively in agreement with this interpretation although the line broadening in O3- $Na_{2/3}Fe_{2/3}Mn_{1/3}O_2$ is around three times smaller as compared with the one observed previously for O3-$Na_{0.9}Ni_{0.45}Mn_{0.55}O_2$ by Cabana et al.[19] Our observations agree with a higher propensity of the O3 structure to disorder but also indicate that the disorder in O3 is strongly reduced when the amount of Na^+ in the structure is reduced and matches the ideal composition of x= 2/3. A similar situation was previously observed when comparing the ^{6}Li MAS NMR line-broadenings in O3- $Li_{0.9}Ni_{0.45}Mn_{0.5}O_2$ and in O3-$Li_{2/3}Ni_{1/3}Mn_{2/3}O_2$. Line-broadening in the second was reduced by approximately 50% due to a reduced extent of structural disorder. It is also possible that the much smaller particle size of the O3-phase (figure 2) has an additional impact in the increased ^{23}Na NMR signal broadening due to lack of structural homogeneity at the surface of the material.

As a conclusion, the solid state NMR data shown in Fig. 4 further confirms the success in the synthesis of pure P2-$Na_{2/3}Fe_{2/3}Mn_{1/3}O_2$ and O3-$Na_{2/3}Fe_{2/3}Mn_{1/3}O_2$ phases and indicates that the amount of structural defects in both materials is rather low, although could be more significant in O3. This observation is important as the presence of defects like stacking faults can result in barriers to ion diffusion and it is expected to have an impact in the electrochemical performance.

The electrochemical cycling curves for P2- and O3-phase are shown in Figures 5a) and b) respectively. P2-phase reached 114.7 mAh/g (0.44 deintercalated Na^+) during the 1st charge and 151.09 mAh/g (0.58 intercalated Na^+) during the 1st discharge cycle within the voltage range of 4.2 – 1.5 V at C/10. At the end of the 1st charge process, 0.22 Na^+ remain in the structure, giving structural support to the layered structure, while at the end of the 1st discharge process, a total of 0.8 Na^+ is found in the interlayer spacing. It is worth noting that approximately 0.14 more Na^+ can be reintercalated into the host material with respect to the pristine material during the 1st discharge process. The end of discharge state of $Na_{0.8}Fe_{2/3}Mn_{1/3}O_2$ indicates that the intercalation of more Na^+ beyond 0.8 into the crystal is hindered probably due to the introduction of Jahn-Teller distortion by reduction of high spin Mn^{4+} to Mn^{3+} (at this concentration the ratio between Mn^{4+} and Mn^{3+} is approximately 0.2:0.13). Indeed, the rapid voltage drop at or below 2.0 V during the discharge process indicates that reintercalation of Na into the crystal structure beyond $Na_{0.8}Fe_{2/3}Mn_{1/3}O_2$ during the discharge is kinetically a hard process due to remarkably strong distortion induced by increasing concentration of Mn^{3+}. The subsequent charge/discharge cycles resulted in cycling of 0.55 – 0.60 Na^+ while a gradual capacity loss is observed. During the 1st charge process, it is clearly visible that $Fe^{3+/4+}$ is the only contributing redox pair with a fairly flat voltage above 3.5 V while during the 1st discharge and beyond, both $Mn^{3+/4+}$ and $Fe^{3+/4+}$ are the contributing redox pairs, with a lower voltage plateau for $Mn^{3+/4+}$.

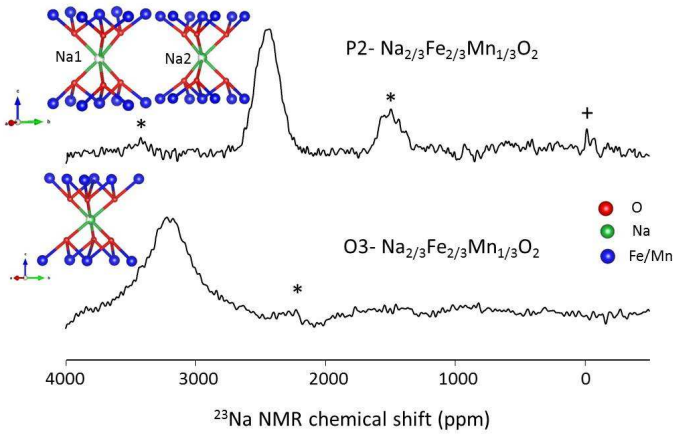

Fig. 4 ^{23}Na MAS NMR spectra of P2-$Na_{2/3}Fe_{2/3}Mn_{1/3}O_2$ and O3-$Na_{2/3}Fe_{2/3}Mn_{1/3}O_2$ acquired at a spinning speed of 50 kHz. The "*" indicates the MAS sidebands of the centerband. Signals marked with "+" correspond to a small fraction of a diamagnetic impurity, presumably Na_2CO_3. Insets show local environments of Na in P2- and O3- $Na_{2/3}Fe_{2/3}Mn_{1/3}O_2$.

O3-phase reached 134.01 mAh/g (0.51 deintercalated Na^+) during the 1st charge and 157.47 mAh/g (0.60 intercalated Na^+) during the 1st discharge cycle within the voltage range of 4.2 – 1.5 V at C/10. When looking carefully at the curve of Fig. 5b into detail, a very small plateau at 2.5V can be observed at the beginning of the first charge process that could be attributed to the presence of a very small amount of Mn^{3+} in the pristine material (estimated value of 0.05 Mn^{3+}). At the end of the 1st charge process, 0.15 Na remain in the structure which means that more Na is deintercalated for O3-phase because the particle size is smaller and therefore, a deeper charge is possible. The amount of extra Na^+ that can be reintercalated into the host structure during the 1st discharge process is slightly smaller (0.09). At the end of the 1st discharge process, the composition $Na_{0.75}Fe_{2/3}Mn_{1/3}O_2$ is achieved, which is similar to the stoichiometry achieved for P2-phase. The subsequent charge/discharge cycles resulted in cycling of 0.55 – 0.60 Na^+ from the crystal. Regardless of end of discharge state, the amount of cycled Na is identical with that of the P2-phase. These results are also very similar to those reported for O3-$Na_{0.82}Fe_{2/3}Mn_{1/3}O_2$ by Delmas' group,[15] for which a very similar capacity was obtained although at a much lower C rate (C/100) and narrower voltage window (1.5 and 3.8 V vs. Na^+/Na).

The electrochemical behaviour of P2- and O3-phases seems thus almost identical as seen in Figure 5. Only slight differences are found for average voltage values and polarization. During the 1st charge process, which corresponds to $Fe^{3+/4+}$ redox process, the average voltage of P2-phase is higher than that of O3-phase and exhibits a larger polarization. Similar trend is observed during the subsequent charge cycles for $Fe^{3+/4+}$ redox process. However, the contrary occurs for the lower voltage plateau which corresponds to $Mn^{3+/4+}$ redox process, for which a lower average voltage and polarization are obtained for P2-phase. Overall the reaction voltages and capacities obtained are however very similar for both materials. On the other hand, different shape of electrochemical curve implies that P2- and O3-phases undergo different reversible phase transitions during cycling, which have been described in previous literature.[8]

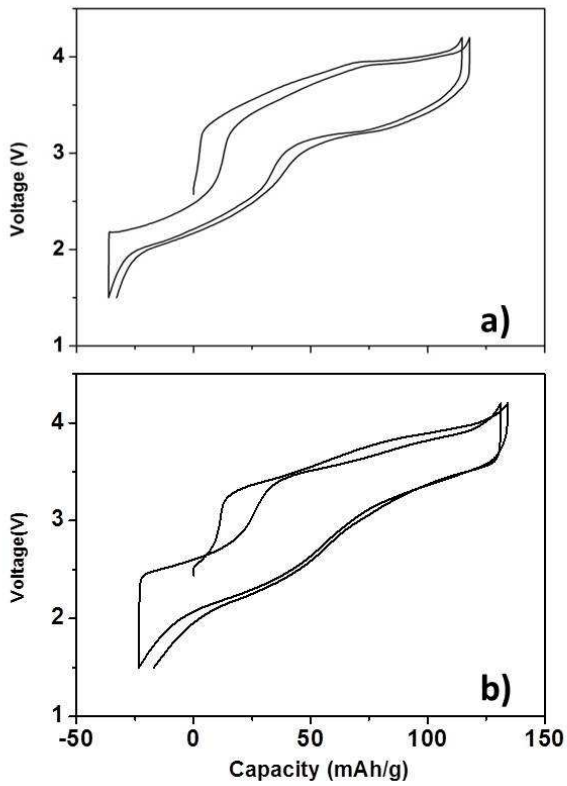

Fig. 5 Comparison of charge-discharge capacity of P2- (a) and O3- (b) $Na_{2/3}Fe_{2/3}Mn_{1/3}O_2$ within the 1st and 2nd cycles.

Ex situ XRDs of both phases stopped at 2.5 V (near OCV of pristine electrode) during the 2nd charge process have been analyzed in order to investigate reversibility of each phase. Fig. 6a clearly indicates that for the P2-phase, the phase obtained at 2.5 V during the 2nd charge process is almost identical to the pristine electrode with hexagonal $P6_3/mmc$ space group and a= 2.9395(1) Å; c= 11.1878(6) Å cell parameters. However, O3-phase obtained at the same voltage value has slightly shifted interlayer peak (001) compared to the pristine electrode with cell parameters of a= 2.9754(4) Å; c= 16.2919(8) Å and rhombohedral R-3m space group, which indicates that the charge/discharge process during the 1st cycle may not be perfectly reversible.

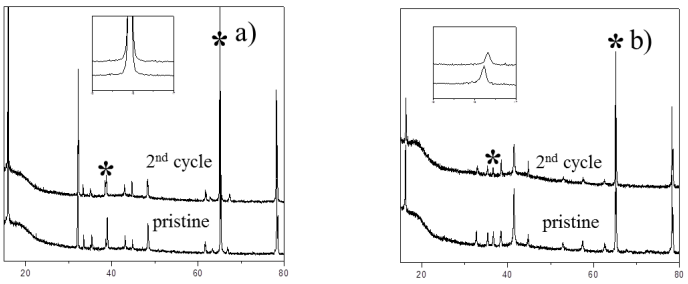

Fig. 6 XRD pastern of pristine and cycled electrode stopped at 2.5 V during the 2nd charge process of (a) P2-phase and (b) O3-phase. Insets are magnified view of interlayer peak (001). Asterisk indicates Al signal from the current collector.

In order to follow the full charge/ discharge mechanism of the P2- and O3- $Na_{2/3}Fe_{2/3}Mn_{1/3}O_2$, *in situ* XRD patterns have been studied and are shown in figures 7a and 7b respectively. A preliminary qualitative analysis of P2- $Na_{2/3}Fe_{2/3}Mn_{1/3}O_2$ data shows a reversible mechanism during the 1st charge/discharge process (see Fig.7a). It starts with a solid solution region from 2.5 V (black line) to 4.0 V (red line), but when OP4-phase appears ((004) diffraction peak at 17.5º illustrated by blue line), a biphasic mechanism is observed up to 4.2 V. During the subsequent discharge process, a solid solution region is found where OP4-phase cell parameters slightly vary when the voltage goes down to 2.5V. A biphasic mechanism is then found between 2.5 V and 1.5 V where OP4- and P2-phase coexist as shown in the green line. However, at 1.5 V, only P2-phase is observed (orange line). When charging up to 2.5 V during the 2nd cycle, which has been considered as reaching the starting point, P2-phase is found to be a unique phase. Such a reversible structural transition is in good agreement with the *ex situ* XRD analysis described above, which is also in good agreement with literature.[8] *In situ* XRD of O3- $Na_{2/3}Fe_{2/3}Mn_{1/3}O_2$ shows a more complicated mechanism with biphasic, triphasic and solid solution regions upon charge and discharge. As shown in fig 7b, during the charge process (from the black line to the blue line) O3-phase undergoes successive phase transition from O3- to P3- and to OP2-phases as reported in previous literature.[20,21] On the other hand, O3-phase exhibits completely different structural transition mechanisms during the discharge process mainly by one biphasic mechanism and a solid solution regime as seen in fig. 7b (blue line to orange line). The phase obtained at 2.5 V during the 2nd charge process (black line) does not have an exactly the same structure as the O3- pristine phase.

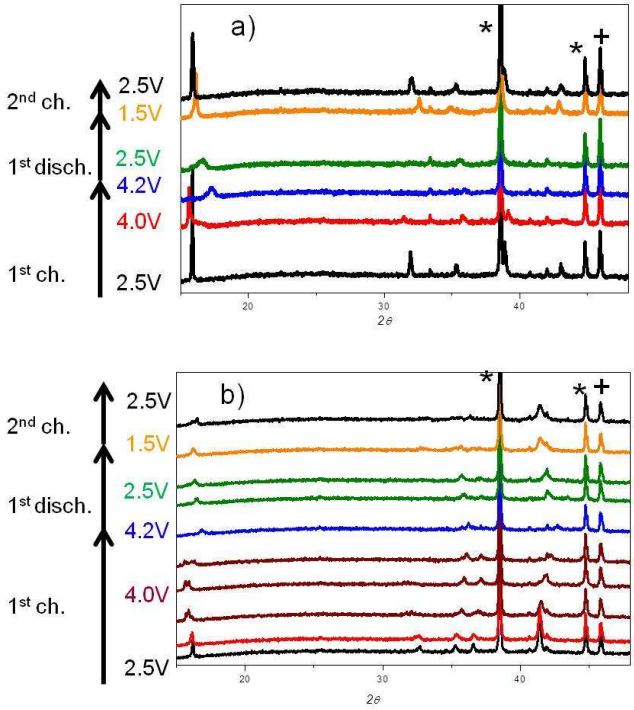

Fig 7 Selected *in situ* XRD patterns of (a) P2-phase and (b) O3-phase. Al and Be signals are pointed with * and + respectively.

As seen in Figures 8a and 8b, a loss of capacity is observed after the first cycle, from 151.09 mAh/g and 157.47mAh/g in the 1st discharge process to 122.83 and 122.24 mAh/g at the 10th cycle for the P2 and O3, respectively. Further cycling shows that the capacity is well kept at similar values up to the 15th cycle. This result reveals that the different oxygen stacking and structural distribution of the cations are not key factors in their electrochemical behavior upon cycling. The difference in the capacity value could be attributed to the different particle size which will facilitate the kinetics as has been previously reported. The gradual degradation of capacity for both compounds is attributed to degradation of electrolyte at high voltage.[15]
Fig. 9a) shows a rate capability study of both phases at C/5, C/7.5, C/5, C/2.5, and 1C rates. At 1C rate, P2-phase exhibits 12.43 % of the 1st

discharge capacity at C/10 while O3-phase exhibits 40.49 % of 1st discharge capacity at C/10.

In figure 9 b) the capacity vs. discharge time is plotted. Evidenced by the shape of curve as the rate decreased to C/10 (36000 s), it appears that the capacity values of both phases converge at infinite time. The smaller particle size of O3 could be one of the possible reasons to explain the different electrochemical behaviour of the two phases as has been previously described.[22]

It has been previously published that P2-phase exhibits better overall electrochemistry comparing to O3-phase[8] because P2-phase possesses better structural stability, and generally P2-phase with prismatic Na environment exhibits better diffusion coefficient than that of octahedrally surrounded Na in O3-phase.[23,24] However, the direct comparison of electrochemistry between P2- and O3-$Na_{2/3}Fe_{2/3}Mn_{1/3}O_2$ shown herein shows that the overall electrochemical performance is almost identical, with better kinetics obtained for O3, which, as mentioned, could be a result of its improved microstructure. Different approaches to decouple the effect of particle size and structure on the kinetics of the studied materials are in progress and will be published elsewhere.

The calculated average voltage considering both $Fe^{3+/4+}$ and $Mn^{3+/4+}$ redox processes is 2.50 V for P2-phase and 2.74 V for O3-phase. Taking into account the capacity values of the first discharge, the energy densities of P2- and O3-phases are 386.05 $mWhg^{-1}$ and 423.878 $mWhg^{-1}$ respectively, which are comparable to those of the lithium layered oxides as $LiMnO_2$ (450 mWhg-1)[25,26] although lower than $Na_{2/3}Fe_{1/2}Mn_{1/2}O_2$ (520 $mWhg^{-1}$)[8].

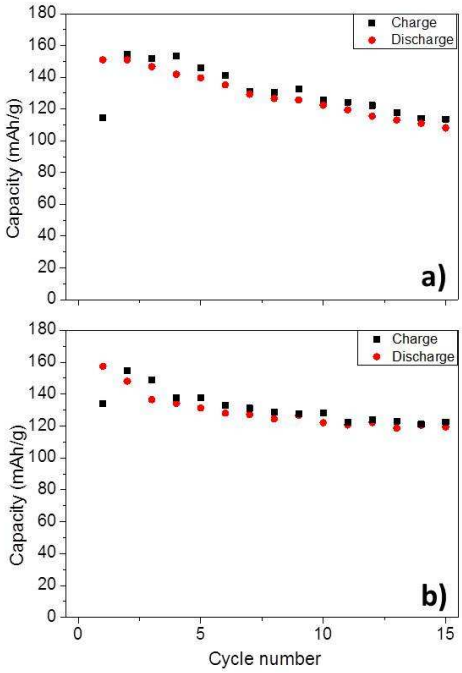

Fig. 8. Cycling stability and the capacity obtained for P2- (a) and O3- (b) $Na_{2/3}Fe_{2/3}Mn_{1/3}O_2$ at C/10 rate after 15 cycles.

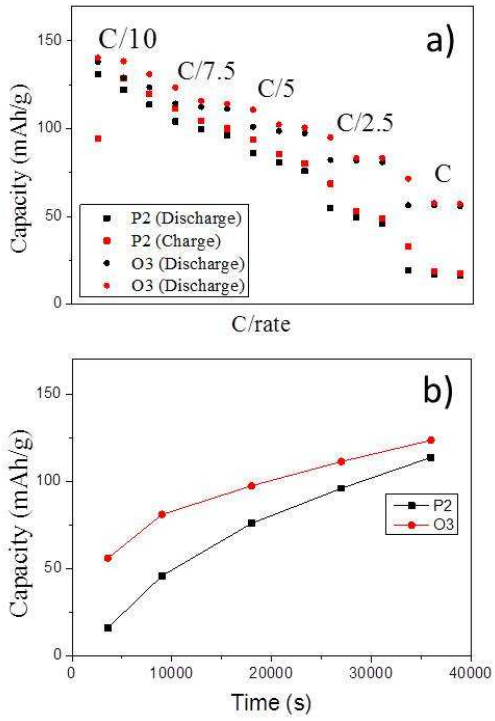

Fig. 9a) Rate capability measurement of P2 (square) and O3 (circle) at successive charge/discharge rate, b) Comparison of the discharge capacity at different C/rates of P2- (black line) and O3- (red line) $Na_{2/3}Fe_{2/3}Mn_{1/3}O_2$.

Conclusions

The synthesis of P2 and O3- $Na_{2/3}Fe_{2/3}Mn_{1/3}O_2$ by using the classical and easy to scale up solid state route has been achieved. Both oxides have the same Fe:Mn cation ratio confirmed by ICP technique. P2- adopts the hexagonal structure with $P6_3/mmc$ space group while the O3-phase adopts the rhombohedral structure with R-3m space group. To our knowledge this is the first time that the two polymorphs are synthesized with the same stoichiometry and their electrochemical performance is directly compared. Initial charge capacities of 114.7mAh/g and 134.01mAh/g are obtained for P2- and O3-phases respectively, within the voltage range of 4.2 - 1.5 V at C/10. The discharge capacity values obtained were 151.09 mAh/g for P2- and 157.47 mAh/g for O3-phase. After 15 cycles the capacity retention of both materials is comparable with a value of 120mAh/g. Although some slight differences in capacity values for both phases in the 1st cycle have been found, it has been demonstrated in this work that both P2- and O3-$Na_{2/3}Fe_{2/3}Mn_{1/3}O_2$ have similar electrochemical performances and suitable energy densities to be used as positive electrode materials for rechargeable sodium batteries. *Ex situ* and *in situ* XRD technique has been utilized to follow the different mechanisms of P2- and O3- phases upon the charge/discharge cycle. In addition, increased rate capability is observed for O3-phase which could be due to smaller particle size.

Acknowledgements

This worked was financially supported by the Gobierno Vasco (ETORTEK CIC ENERGIGUNE 10). The authors thank Dr. Damien Saurel for meaningful discussions.

Notes and references

[a]CICenergigune, Parque Tecnológico de Álava, Albert Einstein 48, ED.CIC, 01510, Miñano, Spain. Tel: +34 945297108.
[b]Departamento de Química Inorgánica, Universidad del País Vasco UPV/EHU, P.O. Box. 644, 48080, Bilbao, Spain. Fax: +34 946013500; Tel: +34 946012458.
*Corresponding Author. E-mail: trojo@cicenergigune.com

[1] J. Goodenough, Y. Kim, *Chem Mat.* 2010, **22**, 587-603.
[2] V. Palomares, P. Serras, I. Villaluenga, K. B. Hueso, J. Carretero-González, T. Rojo, *Energy Environ.Sci.* 2012, **5**, 5884-5901.
[3] V. Palomares, M. Casas-Cabanas, E. Castillo-Martínez, M. H. Han, T. Rojo, *Energy Environ. Sci.,* 2013,**6**, 2312-2337.
[4] P. Vassilaras, X. Ma, X. Li, G. Ceder, *J. Electrochem. Soc.*2013, **160**(12), A207-A211.
[5] X. Ma, H. Chen, G. Ceder, *J. Electrochem. Soc.* 2011, **156**(12), A1307-A1312.
[6] C. Delmas, C. Fouassier, P. Hagenmuller, *Physica*, 1980, **99B**, 81-85.
[7] L.W. Shacklette, T. R. Jow, L. Townsend, *J. Electrochem. Soc.*, 1988, **135**, 2669-2674.
[8] N. Yabuuchi, M. Kajiyama, J. Iwatate, H. Nishikawa, S. Hitomi, R. Okuyama, R. Usui, Y. Yamada, S. Komaba, Nat. Mater., 2012, **11**, 512 – 517.
[9] M. Yoncheva, R. Stoyanova, E. Zhecheva, E. Kuzmanova, M. Sendova-Vassileva, D. Nihtianova, D. Carlier, M. Guignard, C. Delmas, *J. Mater. Chem.* 2012, **22**, 23418-23427.
[10] J. S. Thorne, R. A. Dunlap, M. N. Obrovac, *J. Electrochem. Soc.*, 2013, **160**, A361-A367.
[11] J. Zhao, J. Xu, D.H. Lee, N. Dimov, Y. S. Meng, S. Okada, *J. Power Sources*, 2014, **264**, 235-239.
[12] T. Matsumura, N. Sonoyama, R. Kanno, Solid State Ionics, 2003, **161**, 31-39.
[13] J. Rodríguez-Carvajal, *Physica B.*, 1993, **192**, 55-69.
[14] K. Momma and F. Izumi, *J. Appl. Crystallogr.*, 2011, **44**, 1272-1276.
[15] B. Mortemard de Boisse, D. Carlier, M. Guignard, C. Delmas, *J. Electrochem. Soc.*, 2013, **160**, A569-A574.
[16] M. D'Arienzo, R. Ruffo, R. Scotti, F. Morazzoni, C. M. Maria, S. Polizzi. Phys. Chem. Chem. Phys., 2012, **14**, 5945–5952.
[17] C. P. Grey, N. Dupre, *Chem. Rev.*, 2004, **104**, 4493-4512.
[18] O. H Han.,J. K. Jung,M.-Y. Yi,J. H. Kwak,Y. J. Shin, *Solid State Commun.*, 2000, **117**, 65-68.
[19] J. Cabana, N. A. Chernova, J. Xiao, M. Roppolo, K. A. Aldi, M.S. Whittingham, C. P. Grey, Inorg. Chem., 2013, **52**, 8540-8550.
[20] M. Sathiya, K. Hemallatha, K. Ra,esha, J.M. Tarascon, A.S. Prakash, *Chem.Maters.*, 2012, **24**, 1846-1853.
[21] S. Komaba, N. Yabuchi, T.Nakayarma, A. Ogata, T. Ishikawa, I. Nakai, *Inorg. Chem.*, 2012, **51**, 6211-6220.
[22] J. Wang, J. Polleux, J. Lim, B. Dunn. *J. Phys. Chem. C*, 2007, **111**, 14925-14931.
[23] A. Mendiboure, C. Delmas, P. Hangenmuller. *J. Solid State Chem.*, 1985, **57**, 323-331.
[24] I. Saadoune, A. Maazaz, M. Menetrier , C. Delmas. *J. Solid State Chem.*, 1996, **122**, 111–117
[25] T. Ohzuku, M. Kitagawa, T. Hirai, *J. Electrochem. Soc.* 1990, **137**, 769-775.
[26] Y. Jang, B. Huang, Y. Chiang, D. R. Sadoway, *Electrochemical and Solid-State Letters,* 1998, **1** (1) 13-16.